(2)

FASTC-ID(RS)T-0790-91

FOREIGN TECHNOLOGY DIVISION

TRANSITION INDUCED NORMAL FORCES AND THEIR EFFECTS ON THE AERODYNAMIC CHARACTERISTICS OF SLENDER SHARP CONES

by

Lou Hongtian

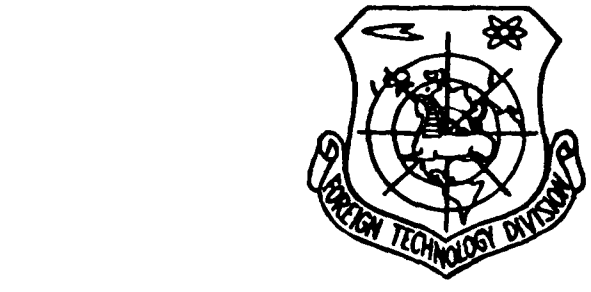

HUMAN TRANSLATION

FASTC-ID(RS)T-0790-91 5 March 1992
#92C000420L

TRANSITION INDUCED NORMAL FORCES AND THEIR EFFECTS ON THE AERODYNAMIC CHARACTERISTICS OF SLENDER SHARP CONES

By: Lou Hongtian

English pages: 31

Source: Yuhang Xuebao, Nr. 3, 1989, pp. 54-64

Country of origin: China
Translated by: SCITRAN
F33657-84-D-0165
Requester: FASTC/TTTAV/J. Michael Phillips, Capt

PREPARED BY:

TRANSLATION DIVISION
FOREIGN TECHNOLOGY DIVISION
WPAFB, OHIO.

GRAPHICS DISCLAIMER

All figures, graphics, tables, equations, etc. merged into this translation were extracted from the best quality copy available.

TITLE: TRANSITION INDUCED NORMAL FORCES AND THEIR EFFECTS ON THE AERODYNAMIC CHARACTERISTICS OF SLENDER SHARP CONES

AUTHOR: Lou Hongtian

ABSTRACT When boundary layers transition, whether or not one has the appearance of induced normal aerodynamic loads is a very significant question. This article introduces static aerodynamic force experiments and dynamic aerodynamic force experiments which were completed in hypersonic wind tunnels. They experimentally verify the existence of this type of load in normal directions. It is created by the asymmetrical nature of boundary layer transitions. In conjunction with this, they have clear and regular influences on the aerodynamic characteristics of long slender cones.

KEY TERMS Boundary Layer Transition, Reynolds Number, Aerodynamic Test, Induced Normal Force

SYMBOLS

C_m, C_{ma}--Pitch moment of force coefficient and its derivative. The latter verifies pitch static stability characteristics. The reference length is d. C_{mq} + C_{ma}--Pitch damping coefficient. Verifies pitch dynamic stability characteristics. C_N, C_{Na}--Normal force coefficient and its derivative. d--Model base radius. L--Model axial length. M, M_{in}, M_{tr} --Pitch moment of force as well as its nonviscous amount and transition induced amount. M, M_∞ --Mach number and, free flow Mach number. N, N_{in}, N_{tr} --Normal force, nonviscous normal force, and transition induced normal force. R_e, R_{eL} --Reynolds number and free flow Reynolds number taking the model length to be the characteristic dimension. $X, \bar{X}$ --Axial distance calculated starting from

the tip of the cone and its ratio with L. X_{cg}, X_{cp}--Location of given center of mass or location of center of vibration, and location of center of pressure. α, $\dot{\alpha}$--Angle of attack and rate of time change. θ_c c(illegible)--Model half cone angle. ω--Frequency of reduction or decrement.

I. INTRODUCTION

When fluids flow past solid wall surfaces, they will produce boundary layers. The transition of boundary layers from laminar flow states to turbulent flow states is an important and complicated problem in fluid mechanics. Since 1883, when Reynolds discovered the phenomenon of transition, a good number of scientists have worked on research into the problem of transition. Going through the work of development in three areas, that is, research into the mechnaisms of transition and its phenomenology, as well as technology for controling the processes of tranistion development, the three of them are complementary to each other's growth. Besides this, development was also done on methods to display transition phenomena and measure them precisely.

55

The discovery and reduction to quantitative measurements of such flow movement phenomena as precisely determined criteria for transition, increases in friction forces on the surfaces of objects after transition, and increases in the rates of heat conduction, have already produced very great influences on the aerodynamic design of flight vehicles, structural design, and trajectory calculations. However, transition's normal loads on the surface of objects as well as the aerodynamic characteristics related to it, such as, normal forces moments of pitch forces, the location of centers of

pressure, and pitch aerodynamic damping, as well as other similar forces, still have a good deal of work which has not yet been carried out on them.

When we went through the use of dynamic testing technology in researching the influences of Reynolds numbers on static and dynamic pitch stability characteristics, we obtained the influences of boundary layer transition on stability parameters of $\theta_c = 10^\circ$ sharp cones and base pressure coefficients [1]. This clearly shows that, when $R_{e(illegible)}$ numbers are relatively low, and transitions are located on the rear body * object surfaces of long slender cones, transitions cause pitch damping to drop, and static stability characteristics increase. When R_e numbers are very high, the location of transition is close to cone tips, and the largest parts of object surfaces are controled by turbulent flow states, static and dynamic stability characteristics almost no longer follow R_e in their changes.

As far as the causes for the appearance of this type of phenomena are concerned, it is recognized that they are the existence, in transition areas, of a transition induced normal force with a direction opposite to nonviscous normal forces[1].

With regard to the concept of transition induced normal forces, it was first seen in Ericsson's article[2]. In the 1960's, the American Ward and others, at the Anode (phonetic) Engineering Development Center's Feng Kamen Laboratory, went through the discovery of the phenomenon that back body transition causes an increase in pitch damping associated with long slender cones. In conjunction with this, it was verified by the laboratories of Uselten[3], Olmsted[4], East[5], and other similar people. Ericcson, in analyzing the causes for the appearance of this type of phenomenon, pointed out that this

is due to the fact that the transitions of laminar layers associated with long slender cones in states at angles of attack are asymmetrical, and that is the reason. The leeward surfaces of laminar flows, under the actions of lateral flow effects and due to accumulations associated with low energy flows, have relatively bad stability characteristics and easily transition. The transition locations are leading in front of the transition locations associated with surfaces meeting the wind. At small angles of attack, (tests verify it at approximately $a \leq 4^{\circ}$), the leading amount is almost in direct proportion with the angle of attack. This is nothing else than what is called asymmetrical transition [4]. The boundary layer displacement thicknesses associated with turbulent flow object surfaces are thicker relative to the states for laminar flows. When angles of attack are relatively small, the effective aerodynamic outside shapes of long slender cones are capable of being simplified into a double cone solid. Its conic surface is formed by the surface of displacement, as is shown in Fig.1. As far as pressure integrals in normal directions for the surface planes of objects with the outside shapes in question are concerned, they are appropriate to the transition induced normal force N_{tr}^{i} which is added in an opposite direction onto the nonviscous normal forces Nin associated with the original long slender cone (not figuring the influence of laminar flow boundary layers).

When angles of attack are small, due to the fact that angular displacements of turbulent flow displacement surfaces relative to the original laminar flow displacement surfaces on the surfaces meeting the wind, the leeward surfaces, and, as a result, on the other meridian surfaces, are almost equal to each other, as a result of it, the amounts of the pressure increases given rise to by transition in most areas are capable of mutually canceling

each other out. The actions of aerodynamic asymmetry, in actuality, only exist on a section of the cone surface in the vicinity of the transtion area (for example, the shadowed area in Fig.1). As a result of this, transition induced normal forces also are certainly in the transition area.

Because of this, it is not difficult to understand that the moment of additional forces lifting the nose, which is supplied by the rear body transition, causes the conic body pitch static stability characteristics to drop. Due to the fact that dynamic models have pitch atitude motions with winding epicenters, boundary layers set up show the appearance of hysterisis lagging effects. The additional moment of forces lifting the nose or pitching moment coupled with attitude motions produce damping effects, causing the dynamic pitch stability characteristics of the conic body to increase. When the forward body transitions, what it supplies is an additional moment of forces lowering the nose. Causing the static stability characteristics to increase drops the dynamic stability characteristics. When the transition moves to the vicinity of the tip of the cone, the asymmetrical transition effects are very small. As a result of this, static and dynamic stability characteristics no longer follow changes in R_e as they alter. This approach explains very well the dynamic experimental results of Reference [1].

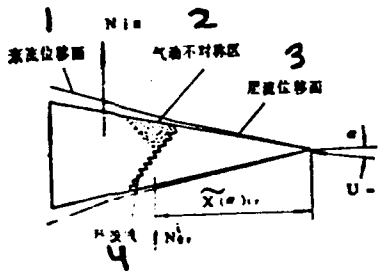

Fig.1 The Concept of Transition Induced Normal Forces (1) Turbulent Flow Displacement Surface (2) Area of Aerodynamic Asymmetry (3) Laminar Flow Displacement Surface (4) Transition Line

However, it should be pointed out that Ward and other similar people obtained experimental results for the stability characteristics of long slender cones as they varied along with changes in R_e numbers and they showed almost no appearance of the influence of the asymmetrical characteristics of forward body transition. Also, what was lacking in even more powerful experimental results in order to verify this type of change was precisely ones given rise to by asymmetrical transitions. (Note: "Forward" and "back" take as their division the center of mass of the flight vehicle or epicenter or center of vibration of dynamic models.) In conjunction with this, using tests to verify the actual existence of this type of tranistion induced normal force had, as a result, the fact that the concept of transition induced normal forces has still not received adequate attention and obtained universal acceptance. 56

In order to verify the actual existence of transition induced normal forces, in conjunction with the fact that they are actually given rise to by asymmetrical transition, as well as to study the effects of the induced normal forces in question on related aerodynamic parameters, we designed a set of dynamic aerodynamic force experiments and obtained thoroughly satisfying results[6]. This article will introduce in relative detail the experimental equipment used in this research as well as the experimental conditions, experimental methods, and the results obtained, in conjunction with which it will carry out an analysis of them.

All the models used in this research are right spherical cones with $\theta_c = 10^\circ$. This is in order to facilitate making comparisons by using the results of previous research as well as the results from the same type

of research done outside of the country. There are two obvious reasons to opt for the use of this model. One is that its outside shape is the most simple. The results of theoretical and experimental research are the most abundant. As a result of this, in the research on aerodynamics, one uses it in order to make standard models for utilization. On the other hand, it is very close to the outside shape of the hypersonic reentry body. The results of research have important value for engineering designs.

II. STATIC EXPERIMENTAL RESEARCH AND ITS RESULTS

The purpose of experiments on static aerodynamic forces is to directly verify by experiment the existence of normal forces induced by transition. In conjunction with this, it is to observe characteristic parameters with respect to static aerodynamic forces, such as the influences on normal forces, moments of pitch forces, pressure centers, and so on.

The first static experiments were completed in wind tunnel #2 of the Beijing Aerodynamics Research Institute. This is a supersonic-hypersonic wind tunnel. The exit areas of the jet tubes which are used in the experiments in question were 20x20 cm^2. The experimental phase nominal Mach number is 5. The overall temperature T_0 = 383 K. The overall pressure P_0 = 0.726 2.55 MP_a. Reynolds numbers were R_{eL} = 2.01 x 10^6 7.20 x 10^6. Models had a base radius of 5. θ_c = 10^o for a right circular cone with a level base. It is constructed with the use of stainless steel. The surface smoothness is V7. The main measurement equipment is No.201 three component water cooled strain type static aerodynamic force balances as well as the corresponding data collection and processing equipment.

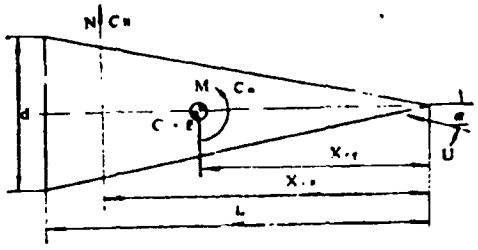

Fig.2 Diagram of Model Coordinate System and Aerodynamic Parameters

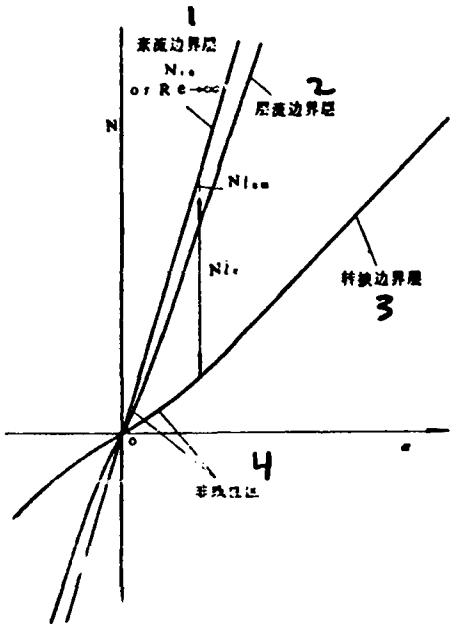

Fig.3 Influences of Laminar Flow States on Normal Forces
(1) Turbulent Boundary Layer (2) Laminar Boundary Layer
(3) Transition Boundary Layer (4) Region of Nonlinearity

Experimental measurements were made of changes in the normal loads, axial loads, pitching moments, as well as base section pressures of models as they followed changes in angles of attack. The range of changes in angles of attack

was a $=-2°\sim10°$, . When angles of attack are small, the interval $\Delta\alpha = 1^{\circ}$. When $a > 6^{\circ}$, $\Delta\alpha = 2^{\circ}$. According to conventional methods, making the change to a dimensionless condition and doing the appropriate conversions, it is possible to obtain the model's normal force coefficient C_N and coefficient C_m for the pitching moment with regard to the given location for the center of mass $X_{..}= 0.652$. The model coordinate system as well as the main aerodynamic parameters can be seen in the diagram in Fig.2.

Experimental data clearly show that, when R_e numbers are relatively low (corresponding to boundary layer transition on the rear body), the changes in normal force N following a, in the vicinity of $a = 0^{\circ}$, are obviously nonlinear. When R_e numbers increase, nonlinearity is reduced. When R_e numbers are very large, one sees almost no nonlinearity phenomena. Moreover, values stay close to ones calculated from nonviscous theory[7]. As far as classical states, such as that in Fig.3, in which there is nonlinearity in the vicinity of zero angles of attack, are concerned, of course, this is drawn out in an exagerated way in order to explain the problem. Actual nonlinearities do not possess this type of severity. Actual data also clearly show that it is most certainly not the case that, the lower R_e numbers are, the more severe nonlinearity is. On the contrary, when R_e numbers are lower than a certain value, nonlinearity is, by contrast, reduced. We also paid attention, in other experimental results, to the fact that, in laminar flow states, long slender cones' $N\sim\alpha$ curves, although showing the existence of nonlinearity, did not, however, show large amounts of it. As a result of this, in the Fig., we also drew out the $N\sim\alpha$ curve corresponding to laminar flow.

From Fig.3, it is not difficult to see that, with angles of attack that are the same, and, when R_e numbers are different (that is, different laminar flow states),

57

normal forces are obviously different. For example, we take the normal forces for long slender cones and see them as being the sum, at times when there are no boundary layers, of normal forces (that is, nonviscous or inviscid normal forces N_{in}) and the amount of induction associated with boundary layers N_v', that is:

$$N = N_{in} + N_v' \tag{1}$$

It is possible to know that the direction of the induced quantities in question is opposite to the direction of the inviscid normal forces. Moreover, because, within the range of R_e numbers in question, even if it is laminar flow states that are located in control positions or turbulent flow states located in control positions, the influence of viscosity is small in all cases. It is possible to imagine that the induced quantities in question are primarily induced by boundary layer transition, that is, their principal component is the boundary induced quantity N_{tr}'. The dimensionless coefficient is $(C_N)_{tr}'$. In this way, equation (1) is capable of being expressed as:

$$N \cong N_{in} + N_{tr}' \tag{2}$$

Or using coefficients, it is capable of being expressed as:

$$C_N \cong (C_N)_{in} + (C_N)_{tr}' \tag{3}$$

This just verified that, when boundary layers are in a transtion flow state, one actually has the existence of transtion induced normal forces which are opposite in direction to inviscid normal forces.

Normally, one uses aerodynamic quantities with a = 0° in order to represent the aerodynamic characteristics in the vicinity of small angles of attack. In order to lower the influence of probable errors, we used minimum square laws to draft up straight lines for the various individual C_N and C_m values at a = -2°, -1°, 0°, 1°, and 2°.
After that is done, one solves for the angles of attack, obtaining the normal force coefficient derivative C_{Na} for zero angle of attack, and the pitching moment of force coefficient derivative C_{ma} as well as the pressure center coefficient X_{cp} as obtained from the equation below for a = 0°.

$$X_{cp} = X_{cg} - \frac{d}{L}\frac{C_{ma}}{C_{Na}} \tag{4}$$

C_{Na}, C_{ma}, and $\bar{X}_{cp}$ change along with R_e numbers in ways that are respectively represented in Fig.'s 4, 5, and 6. Each data point is the arithmetic mean value of experiments repeated twice.

From Fig.4, it is possible to know that, when R_e numbers are very low, C_{Na} is relatively large. When R_e numbers increase, C_{Na} drops. In conjunction with this, R_{eL} drops to a small value of $R_{eL} \cong 3.4 \times 10^6$.
Following along with continued increases in R_e, C_{Na} increases, and, in conjunction with that, gradually tends toward a constant value. This constant value is close to the Sims theoretical value[7]. The Fig.'s in question clearly show that $C_{Na} \sim R_{eL}$ curves, in the interval of medium range R_e numbers, show the existence of obvious valley areas. The reason for this is that there is no relationship between inviscid values and R_e numbers. Moreover, the influences of the values of R_e numbers on

58

values at times of laminar flow states and turbulent flow states are also very small. Comparing Fig.3, it is not difficult to reach the conclusion that the appearance of the valley areas in question just happen to clearly show the existence of transition induced normal forces as well as the rules or patterns in the changes which follow R_e numbers.

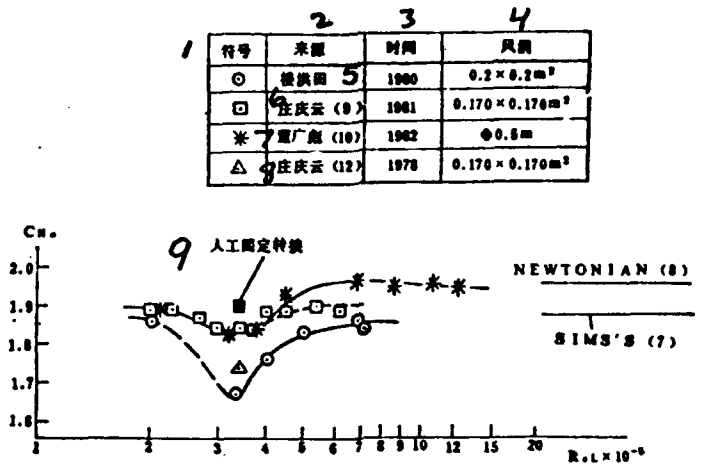

Fig.4 Changes in Normal Force Coefficient Derivatives Following R_e Numbers (1) Symbol (2) Source (3) Time (4) Wind Tunnel (5) Lou Hongtian (6) Zhuang Qingyun (7) Dong Guangbiao (8) Zhuang Qingyun (9) Artificially Fixed Transition

As far as the characteristics discussed above for changes in normal force coefficient derivatives following along with R_e are concerned, they are also verified by static aerodynamic force experiments[9.10] of a similar type which were completed shortly afterwards. In order to make comparisons, the results of them were also sketched on the corresponding Fig. From Fig.4, it is possible to know that the results from the references [9.10] and the changes in normal force coefficient derivatives which follow

along with R_e numbers, in all cases, have the same type of valley shaped characteristic as the results from our tests. Moreover, the R_e numbers positioned at the bottoms of the valleys also approach each other. This just more strongly verifies that transition induced normal forces really do exist. Also, their changes following along with R_e numbers are regular.

Zhuang Qingyun[9] also, at the same time, made an artificially fixed transition test. He, at a spot approximately $\bar{X} = 0.1$ away from the front end of the model, used small plastic balls with $d = 0.3 \sim 0.4$ mm to create a viscous band of roughness 5 mm wide. This makes the boundary layer at that spot form a symmetrical transition. The results clearly showed that the experimental values which were obtained for normal force coefficient derivatives and very, very high or very, very low R_e numbers approached each other. Moreover, there was a clear difference from natural transition values with the same R_e numbers. This also verified that transition induced normal forces are produced by asymmetrical transitions.

Fig.5 is experimental values for changes in coefficient derivatives following along with R_e numbers. In order to make comparisons, also, in the same way, we sketched in the experimental values of Zhuang Qingyun and Dong Guangbiao. Besides this, we sketched in the results for dynamic experiments from Reference [1] and the results from dynamic experiments from this article.

From the Fig., it is possible to know that, from three wind tunnels, at different times, using different methods and different test measuring equipment, the data points obtained, in all cases, regularly lay within a band of data. This band of data clearly shows that, when R_e numbers are relatively low, the pitch stability characteristics for long slender cones are relatively low, and, in conjunction with

this, one has the appearance of valley values with a certain R_e number. When R_e numbers are relatively high, stability characteristics increase, and, in conjunction with that, one has the appearance of peak values. When R_e numbers are adequately high, stability characteristics drop. The latter approach very closely to inviscid theoretical values.

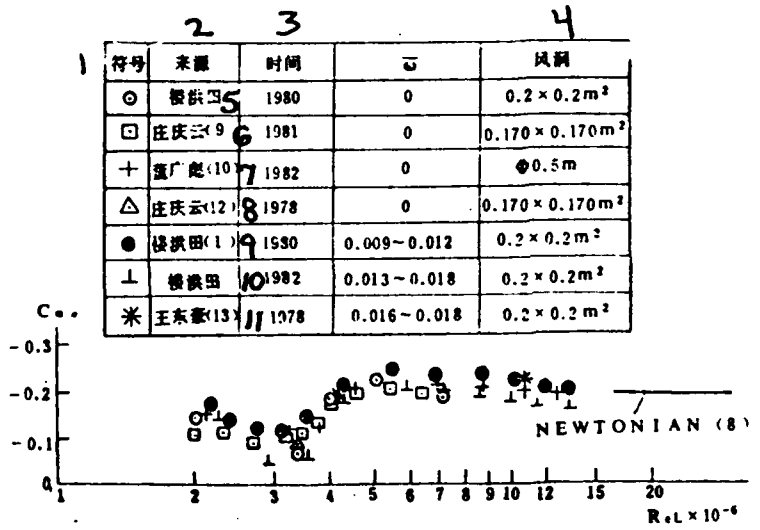

Fig.5 Changes in Pitch Moment of Force Coefficient Derivatives Along With R_e Numbers (1) Symbol (2) Source (3) Time (4) Wind Tunnel (5) Lou Hongtian (6) Zhuang Qingyun (7) Dong Guangbiao (8) Zhuang Qingyun (9) Lou Hongtian (10) Lou Hongtian (11) Wang Donghao.

Fig.6 is the changes in pressure coefficients following along with R_e numbers obtained from calculations with the results on models for three static state experiments discussed above. It clearly shows that, when R_e numbers are relatively low, viscous pressure centers exist before inviscid pressure centers. Moreover, the amount of forward displacement is quite large. The largest amount of

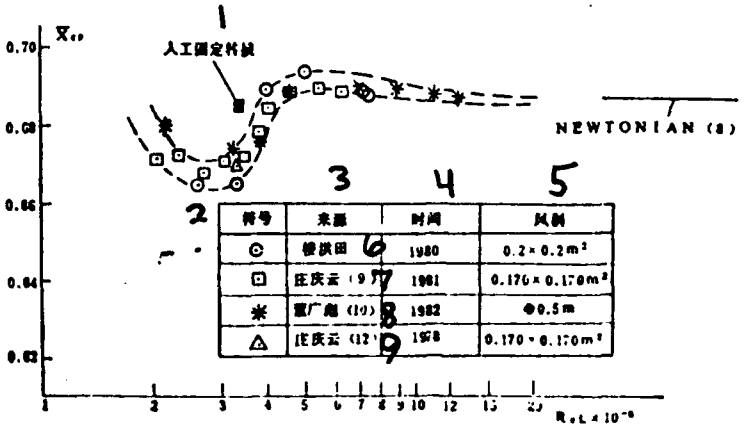

Fig.6 Changes in Pressure Center Coefficients Following Along With R_e Numbers (1) Artificially Fixed Transition (2) Symbol (3) Source (4) Time (5) Wind Tunnel (6) Lou Hongtian (7) Zhuang Qingyun (8) Dong Guangbiao (9) Zhuang Qingyun

forward displacement reaches approximately 2% of the entire length of the model. When R_e numbers are relatively large, viscous pressure centers move to areas slightly behind inviscid pressure centers. When R_e numbers are relatively large, viscous pressure centers approach inviscid pressure centers. Inviscid pressure centers are given in accordance with Sims theoretical values[7] or Newtonian theoretical values[8] and are:

$$(X_{cp})_{in}=\frac{2}{3}(1+\lg^{3}\theta_{c})=0.6874 \qquad (5)$$

III. DYNAMIC EXPERIMENTAL RESEARCH AND ITS RESULTS

Static experimental results already verify the

existence of transition induced normal forces. In conjunction with this, they precisely determine general rules or patterns influencing the aerodynamic characteristics of long slender cones from the induced normal forces in question. The artificial transition experiments in the static tests of Zhuang Qingyun and the dynamic experiments of Reference [1] have also already initially verified that aerodynamic asymmetries at the time of natural transitions are the principal cause forming transition induced normal forces. In order to even more powerfully prove that transition induced normal forces come from asymmetrical tranisitions, we designed a set of relatively complete dynamic tests. We are capable of assuring that, since transition induced normal forces are created by aerodynamic asymmetries which form at the time of natural boundary layer transition, then, using artificial transition methods to make boundary layers, at a fixed location, show the appearance of symmetrical transition, then, one will not have the appearance of the various types of phenomena associated with changes in aerodynamic characteristics following along with R_e numbers. As a result, this will, then, also clearly demonstrate that, when transitions are symmetrical, one will not have the appearance of transtition induced normal forces.

In these experiments, the models which were used were still right circular cones with flat bases and θ c(illegible) $= 10^{\circ}$. d = 7 cm. Centers of vibration were set at the location of the given center of mass, the position $X_{..}$ = 0.632. The experiments, in the same way, were completed in the #2 wind tunnel discussed above. M = 5. The overall temperature of gas flow T_0 = 373 K. The overall pressure p_0=0.49~3.33MPa . The Reynolds numbers were R_{eL}=2.30×10⁶~13.4×10⁶. The dynamic balances used were still the No. 401 single degree of freedom, small amplitude, free pitch vibration dynamic derivative balance. Its operating principles can be seen in

Reference [1]. The range of amplitude changes is $\theta = \pm$ 3°~±1° The frequency of reduction or contraction ω = 0.013 0.018.

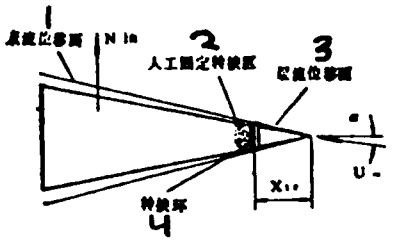

Fig.7 Artificially Fixed Symmetrical Transition (1) Turbulent Flow Displacement Surface (2) Artificially Fixed Transition Area (3) Laminar Flow Displacement Surface (4) Transition Ring

The model used was created with an aluminum alloy. The surface smoothness was ▽6. When carrying out artificial transition experiments, at a position X_{tr} = 0.2 away from the end point, a metal ring made from two red copper wires with a diameter of 0.5 mm adheres to act as a fixed transition ring in order to force boundary layers at this place to form symmetrical transitions such as those in Fig.7.

The basic principles of dynamic experiments and data processing procedures are completely the same as those in Reference [1]. After obtaining frequency parameters and vibration pattern attenuation coefficients, it is then possible to obtain model pitch force moment derivative M_α and pitch damping derivative $M_{\dot{\alpha}}$. After that, from the equations set out below, one obtains pitch force moment coefficient derivatives and pitch damping coefficients

$$C_{m_\alpha} = \frac{4}{\pi d^3 q_\infty} M_\alpha \qquad (6)$$

$$C_{mq}+C_{m\dot{\alpha}}=\frac{4M_\infty a_\infty}{\pi d^2 q_\infty}M_i \qquad (7)$$

In these equations, $M_\infty, q_\infty, a_\infty$, respectively, are the free flow Mach number, dynamic pressure head, and the speed of sound.

The experimental results are as seen in Fig.8. In the Fig., each data point only represents one iteration of experiments. If one is capable of making an appropriate number of repeated experiments, the regular nature of data may possibly be a good deal better.

From the Fig.'s, it is possible to know that the results for conditions of natural transition are extremely similar to the experimental results introduced in Reference [1]. Following along with R_e numbers, they present the appearance of changes which are clear and regular. The absolute values of the two results have a small amount of difference between them. This is primarily created by differences in the dimensions of holes opened in the base section. As far as the experiments in Reference [1] are concerned, the ratio for holes opened in the base section was $d_o/d = 0.500$. For these experiments, it was 0.914. In these, d_o was the diameter of holes in the bases. Research clearly shows that, with regard to dynamic experiments, when the rear body surface is placed in a transition flow state, the opening of holes in the base section has a relatively obvious influence. Research results were published in Reference [11]. Of course, due to the different elasticities of components, a result was that the reduction or decrement frequencies were different, and this will also have an influence.

There are obvious differences between the results for artificial transition and the results for natural transition. Fig.8 clearly shows that, when symmetrical

transition is formed, the stability of long slender cones no longer is related to R_e numbers. One no longer sees the appearance of changes in natural transtion phenomena associated with patterns of regularity presented following along with R_e numbers. This correlated experimentation clearly proves that, under conditions of symmetrical transition, transition induced normal forces no longer exist.

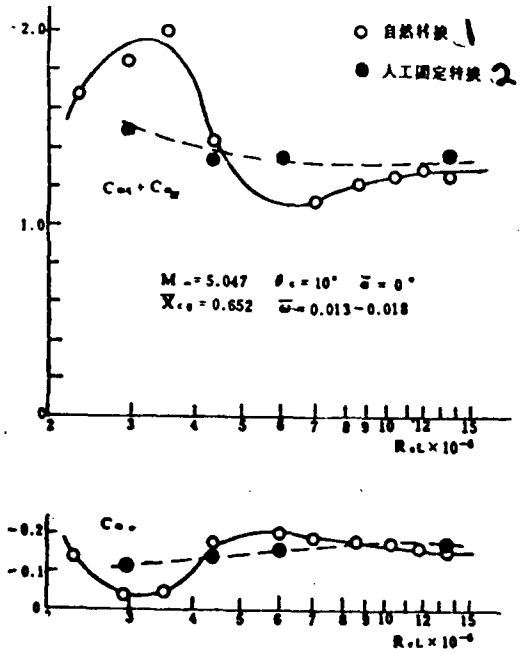

Fig.8 A Comparison of Results for Natural and Artificial Transtion (1) Natural Transition (2) Artificial Fixed Transition

From Fig.8, it is possible to know that, in artificial transition, stability following along with R_e numbers still has a good deal of variation associated with it. It is possible to see that, when R_e numbers are relatively low, pitch dynamic stability characteristics are relatively

great. In conjunction with this, they follow along with increases in R_e numbers and gradually decrease. Finally, they tend closely toward inviscid experimental values. The changes associated with the static pitch stability characteristics are, by contrast, just the opposite. They, from the relatively small values associated with low R_e numbers, follow along with increases in R_e numbers and gradually increase. In conjunction with this, they gradually tend closely toward inviscid experimental values. Different from times of natural transition, not only are the amplitude values of changes small. Moreover, changes are monotonic. They do not show the appearance of peak or valley value phenomena. The reason for the appearance of this type of phenomena is because artificial transition occurs at conditions of relatively low R_e numbers. As a result of this, compared to the object surfaces associated with natural transition, boundary layer displacement thicknesses are relatively large, and this is the reason viscosity effects are relatively strong. This type of phenomena will also appear in states of simple laminar flow or simple turbulent flow.

IV. ANALYSIS AND DISCUSSION

In the previous discussion, we have already introduced the concept of transition induced normal forces. Static aerodynamic experimentation has already demonstrated the existence of transition induced normal forces and their characteristic of following R_e numbers in presenting valley shaped variations. How transition induced normal forces follow R_e numbers and present valley shaped variations is capable of being understood as follows.

Reference [1] has already clearly proven that, in the interval of R_e numbers associated with our experiments, the flow states on the object surfaces of long slender cones are placed in a state of transition. Moreover, the area of transition follows R_e numbers and increases, gradually moving close to the tip of the cone. A good number of experiments have already verified that transition is not completed instantaneously. On the surface of objects, there exists a relatively long area of transition development. The length of the area in question and the distance from that area to the tip of the cone form a ratio or proportion. Fig.1 is only one type of simplified method of representing it. The actual situation, of course, must be much more complicated. Fig.4 clearly shows that, when $R_{eL} \cong 3.4 \times 10^6$, the C_{Na} curve is positioned at the bottom of the valley, that is, the value at which normal forces associated with viscous cones show their appearance at a minimum. To say it another way, the induced normal forces show the appearance of a maximum value. When R_e numbers increase or decrease, transition induced normal forces gradually get smaller. Comparing Fig.9 from Reference [1], it is possible to know that, when $R_{eL} \cong 3.4 \times 10^6$, transition shows its appearance in the vicinity of $\bar{X} = 0.7$. It exists in an angle of attack state. At this time, asymmetrical transition zones occupy the maximum surface area. As a result of this, asymmetrical aerodynamic effects are the most clear, forming the maximum transition induced normal forces. R_e numbers increase, and the transition location moves forward. The transition zone shortens. The diameter of the area in question is also relatively small. As a result of this, asymmetrical aerodynamic effects are weak. Transition induced normal forces lessen. When R_e numbers are adequately large and object surfaces are primarily controled by turbulent boundary flows, viscosity effects are very small. Moreover, basically, one does not have the

appearance of asymmetrical aerodynamic effects. As a result of this, transition induced normal forces disappear. Normal force coefficient derivatives associated with viscous cones come close to inviscid values. Conversely, when R_e is lower than 3.4×10^6, transition areas move even closer to locations at the base of cones. At this time, although transition zones should be even longer, because they are too close to the base of the cones, however, they normally cannot form complete transition processes. Transition areas associated with the surfaces of cones, on the contrary, shorten. Moreover, because they are too close to the base of cones, the pressure discharge effects toward the low pressure areas at the base of the cones are strong. As a result of this, asymmetrical effects are weak. Transition induced normal forces lessen.

When using coarse bands to form symmetrical transition, because one no longer has the existence of asymmetrical aerodynamic effects, as a result of this, one will then also no longer have the appearance of transition induced normal forces any more. Because of this, from Fig.4, it is possible to see that, when transition is artificial, the values associated with normal force coefficient derivatives and the values associated with times when R_e numbers are very large approach each other. 61

As far as verifying the existence of transition induced normal forces and the rules or patterns for their changes following along after R_e numbers is concerned, it is then possible to easily explain the patterns or rules for the changes in pitch force moment coefficient derivatives and pressure center coefficients following along with R_e numbers as presented in Fig.5 and Fig.6.

On the basis of equations (2) and (3), as well as Fig.2, for the moment of pitch forces associated with the center of mass, it is possible to express it as being:

$$M=-(X_{cp}-X_{cg})N=M_{in}+M_{tr} \tag{8}$$

In this,

$$M_{in}=-[(X_{cp})_{in}-X_{cg}]N_{in} \tag{9}$$

$$M_{tr}=-[\bar{X}(a)_{tr}-X_{cg}]N_{tr} \tag{10}$$

Or, using dimensionless quantities to express it, one has:

$$C_{ma}=-\frac{d}{L}(X_{cp}-X_{cg})C_{Na}=(C_{ma})_{in}+(C_{ma})_{tr} \tag{11}$$

$$(C_{ma})_{in}=-\frac{d}{L}[(X_{cp})_{in}-X_{cg}](C_{Na})_{in} \tag{12}$$

$$(C_{ma})_{tr}=-\frac{d}{L}\left[\bar{\bar{X}}(a)_{tr}-X_{cg}\right](C_{Na})_{tr} \tag{13}$$

In the various equations set out above, $\bar{X}(a)_{tr}$, under angle of attack states, is the average distance from the transition location to the tip of the cone. When the angle of attack tends toward zero, the values in question will somewhat increase.

From the various equations set out above, it is possible to know that, at times of rear body transition, $\bar{X}(a)_{tr}>X_{cg}$. Transition induced normal forces produce pitching moments, that is, $M_{tr}>0$. This offsets the partial stability effects associated with inviscid normal forces, causing the static stabilities of cone bodies to drop. Due to the fact that the pitching moment in question

M_{tr} is the product of the transition induced normal forces and the distance between the point of effect of the forces in question and the center of mass, because of this, even though $R_{eL} < 3.4 \times 10^6$, the transition induced normal forces have already gotten smaller. However, due to the fact that the effects of the lengthening of the distance are even more obvious, as a result of this, at relatively low R_e numbers, it is still possible to have the appearance of even larger instability effects. This is nothing else than the reason why, in Fig.5, stability valley values, as compared to the valley values for the normal force coefficient derivatives of Fig.4, show the appearance of even lower R_e numbers. When R_e numbers are relatively large and transition moves to the front of the object surface, $\bar{X}(a)_{tr} < X_{cg}$, . $M_{tr}^{i} < 0$. This supplies the moment of forces for lowering the nose, causing the stability characteristics of cone bodies to increase. In conjunction with this, on the appropriate forward bodies, transition locations reach peak values. After this is the case, they gradually return to normal. In conjunction with this, they tend toward inviscid values.

On the basis of equations (11), (12), and (13), pressure coefficients associated with transition cones are capable of being expressed as:

$$\frac{X_{cp}}{(X_{cp})_i} = \frac{(C_{N\alpha})_{in} + [\bar{X}(a)_{tr}/(X_{cp})_{in}](C_{N\alpha})_{tr}}{(C_{N\alpha})_{in} + (C_{N\alpha})_{tr}} \qquad (14)$$

Because the directions of transition induced normal forces and the directions of inviscid normal forces are opposite to each other, when R_e numbers are relatively low and transition locations are situated in the lower reaches of

inviscid pressure centers, that is to say, $\bar{X}(a)_{tr} > (X_{cp})_{in}$, from equation (14), it is possible to know that one has $X_{cp} < (X_{cp})_{in}$. From Fig.6, it is possible to see that the locations of pressure centers associated with transition cones very clearly move to the upper reaches of inviscid pressure centers. Conversely, when R_e numbers are relatively high and transition moves to the upper reaches of inviscid pressure centers, that is to say, $\bar{X}(X)_{tr} < (X_{cp})_{in}$, from equation (14), one has, $X_{cp} > (X_{cp})_{in}$. In Fig.6, what is displayed is the location of transition cone pressure centers, as compared to inviscid pressure centers, having a slight amount of backward movement. When R_e numbers are very high, $\bar{X}(a)_{tr}$ and $(C_{Na})_{tr(illegible)}$ are both very small. As a result of this, from equation (14), one knows that $X_{cp} \cong (X_{cp})_{in}$. In Fig.6, by contrast, one has shown the appearance of viscous cone pressure centers approaching toward inviscid pressure centers. From this, it is possible to know that the concept of transition induced normal forces explained very well the patterns or rules for changes in pressure coefficients of long slender cones following along with R_e numbers.

The changes in pitch damping following along with R_e numbers as displayed in Fig.8 are then given rise to by the coupling of additional moments of force formed by transition induced normal forces and the pitch attitude movements of long slender cones. A detailed explanation of changes following along with R_e numbers is seen in Reference [1].

To summarize what has been described above, speaking in terms of long slender cones and due to the fact of the existence of transition induced normal forces, the general rules or patterns for the various aerodynamic characteristic parameters related to them following along with R_e numbers are capable of being shown in Fig.9.

62

From Fig.'s 4, 5, and 6, it is possible to see that, between three static state experiments, not only does the data for changes following along with R_e numbers tend to be the same. Moreover, in terms of quantitative values, they are also very close. Among these, the band width of distribution for the numerical data points associated with pressure center coefficients X_{cp} are within $\pm$ 0.4%. Normal force coefficient derivatives C_{Na} exist at average values of within $\pm$ 3.4%. Pitch force moment coefficient derivatives C_{ma} exist within average values of approximately $\pm$10%. The consistency of the three experimental results, of course, is, first of all, due to the fact that this type of change tends to be a type of objective reality. It is not a type of coincidental phenomenon. In turn, this also explains the fact that these three types of experiments all have been done relatively successfully.

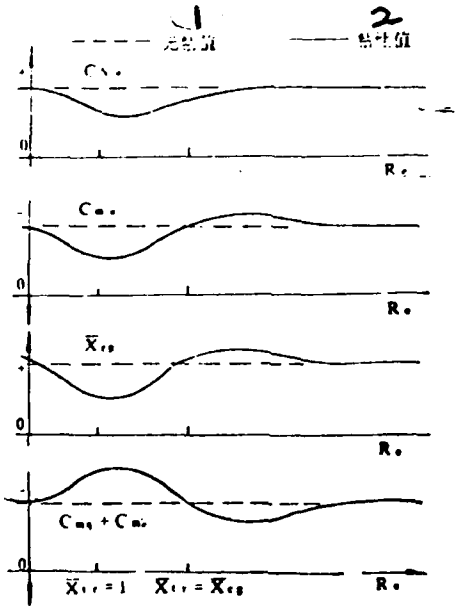

Fig.9 General Rules or Patterns for Changes in Various Aerodynamic Parameters Following Along with R_e (1) Inviscid Value (2) Viscous Value

In these experiments, the precision of the instruments which were used was relatively high. Use was made of programming with full loads, aerodynamic force balances, pressure sensor devices, temperature sensor devices, as well as data collection systems, and, in all cases, they were within $\pm 0.3\%$. However, it should be pointed out that, due to the fact that the actual Mach numbers associated with the the various wind tunnels were not completely the same, the instrument calibration systems and calibration methods were different. This is particularly the case with measurements of aerodynamic forces in the vicinity of zero angles of attack, and normal forces, as well as moments of pitch forces, and angles of attack, which were, in all cases, small quantities. Relative errors were comparatively large. As a result of this, the need to obtain accurate pressure center coefficient derivatives, moments of pitch force coefficent derivatives, and normal force coefficient derivatives will, just basically, be a very difficult thing to do.

Looking at the degree of dispersion of the data points associated with pitch force moment coefficient derivatives, it is relatively large, reaching approximately 10%. This is actually due to the fact that it is calculated relative to the center of mass location $\bar{X}_{.,} = 0.652$. The relative distance $\overline{\Delta X}$ between the point in question and the inviscid pressure center $\bar{X}_{.,} = 0.6874$ is only 3.5%. At times of rear body transition, the relative distance between it and the actual pressure center is only approximately 1.4%, and is very small. As far as very small errors in the measurements of pressure center locations are concerned, in all cases, they will lead to very large relative errors in C_{ma}. From calculations, it is possible to know that the $\pm 10\%$ data dispersion associated with C_{ma}, certainly does not exceed the influences created by the $\pm 0.4\%$ divergence for locations of pressure centers.

From Fig.5, it is possible to know that the results of dynamic experiments and the results of static experiments match up very well with each other. Besides this, a static experimental data point from an early period[12] and different original numerical data from a dynamic test[13] had two data points calculated for pitch force moment coefficient derivatives, and they also fell very well within the data band discussed above.

Of course, if conditions permit, it is possible to select for use an appropriate aerodynamic force balance carrying small amounts in association with small angles of attack. In conjunction with this, with the same experimental conditions and data processing methods (In the three static experiments discussed above, data processing methods were not entirely the same. When solving for aerodynamic derivatives at a zero angle of attack, what Zhuang Qingyun[9] used were methods in which $a = -2^{\circ}$ and $a = +2^{\circ}$ values acted as linear solutions for slope. What Dong Guangbiao[10] used were methods in which values with $a = -4^{\circ}$, -2°, 0°, 2°, and 4° were drafted up, on the basis of minimum or least square methods, to form linear derivations.), and, in intervals with angles of attack contracted to the vicinity of $a = 0^{\circ}$, numerous measurements were made of a number of data. After that, using multiple equations to draft up experimental curves, one again solves for zero angle of attack derivatives. It is certainly possible to obtain even more reliable data. In conjunction with this, one takes another step toward contracting the width of data distribution.

V. CONCLUSION

On the basis of experimental research discussed above, at least with regard to hypersonic flow speeds in long slender cones, it is possible to reach the following conclusions.

(1) At times when the boundary layers associated with the object surfaces of long slender cones are in natural transition states, transition induced normal forces exist. The normal forces in question are created as a result of the asymmetrical characteristics of boundary layer transitions associated with leeward surfaces and surfaces facing into the wind. Their directions are opposite to the directions of inviscid normal forces. The points of the effects are in the transition zones.

63

(2) At times when transitions are positioned on object surfaces slightly in front of base sections, one has the appearance of maximum transition induced normal forces. When R_e numbers are higher or lower than the R_e numbers that correspond to the states discussed above, transition locations move forward or move backward, leading to the lessening of transition induced normal forces. Curves for the changes in the angle of attack derivatives associated with transition induced normal force coefficients versus R_e numbers possess valley shaped characteristics.

(3) At times when R_e numbers are relatively low and transitions are positioned on object surfaces of rear bodies, transition induced normal forces cause pitch dynamic stability characteristics to obviously increase. Pitch static stability characteristics obviously decrease. In conjunction with this, under R_e number conditions which are slightly lower than those at which one has the appearance of maximum transition induced normal forces, one respectively, has the appearance of peak values and valley values. Dropping R_e numbers a step further, stability characteristics will gradually return to normal. At times when R_e numbers are relatively high and transition is located on the object surfaces of forward bodies, transition induced normal forces cause pitch dynamic stability

characteristics to decrease somewhat. Pitch static stability characteristics increase slightly. In conjunction with this, with specific R_e numbers, one respectively has the appearance of peak values and valley values. Taking another step in increasing R_e numbers, stability characteristics will gradually return to normal. In conjunction with this, they will finally tend closely toward inviscid values.

(4) At times when transitions are located on object surfaces in the lower reaches of inviscid pressure centers, transition induced normal forces cause the locations of pressure centers associated with conic bodies to clearly move forward from inviscid pressure centers. After arriving at the most forward positions, following along with another step in the lowering of R_e numbers, they will gradually return to normal. At times when transition is located on object surfaces in the upper reaches of inviscid pressure centers, transition induced normal forces cause pressure center positions to move slightly backward from inviscid pressure centers. After arriving at the most rearward positions, following along with another step in the increasing of R_e numbers, they will gradually return to normal. In conjunction with this, they return in the end to inviscid pressure center locations.

(5) At times when artificial transition methods are used to destroy asymmetrical characteristics of transition, transition induced normal forces no longer exist. Various aerodynamic parameters also no longer follow R_e numbers and present the appearance of obvious and regular variations.

REFERENCES

[1] Lou Hongtian; "The Influences of Boundary Layer Transition on the Static and Dynamic Stability Characteristics of Long Slender Cones", Acta Astronautica Sinica, No.1, 1985

[2] Ericsson, L.E., AIAA 69—106
[3] Cyran, F.B., AEDC-TR-80-17
[4] Ericsson, L.E., AIAA 73—126
[5] East, R.A., AGARD-CP-235, 1978
[6] Lou Hongtian et al, Proceedings of the International Conference on Fluid Mechanics (Supplement), Beijing, 1987
[7] Sims, J.L., NASA SP-3007, 1964
[8] Fisher, L.R., NASA TND-149, 1959

[9] Zhuang Qingyun; "Empirical Research on the Influences of R_e Numbers on the Aerodynamic Characteristics of Sharp Cones", Bulletin of the Beijing Aerodynamics Research Institute, 1981

[10] Dong Guangbiao; "Experimental Research on the Influences of Laminar Surface Transition on the Aerodynamic Characteristics of Sharp Cones", Bulletin of the China Aerodynamics Research and Development Center, 1982

[11] Lou Hongtian; "Influences of Opening Holes in the Base Section of Models on Dynamic Experimental Results", Aerodynamics Journal, Vol.4, No.2, 1986

[12] Zhuang Qingyun; "Second Period of Force Measuring Experiments on Sharp Cone Models in the FD-03 Wind Tunnel", Bulletin of the Beijing Aerodynamics Research Institute, 1979

[13] Wang Donghao; "Concurrent Experimental Reports on 401 Dynamic Pitch Derivative Balance Dynamic Calibration and Sharp Cone Models with Half Cone Angles of 10°", Bulletin of the Beijing Aerodynamics Research Institute, 1978